AD_____

AWARD NUMBER: W81XWH-05-1-0491

TITLE: Non-Invasive Phosphorus-31 Magnetic Resonance Spectral Characterization of Breast Tissue Anomalies Using Pattern Recognition and Artificial Intelligence

PRINCIPAL INVESTIGATOR: Jerry A. Darsey, Ph.D.
Diana Lindquist, Ph.D.
Dan Buzatu, Ph.D.
Ronald Walker, M.D.
Steven Harms, M.D.

CONTRACTING ORGANIZATION: University of Arkansas at Little Rock
Little Rock, Arkansas 72204-1099

REPORT DATE: August 2006

TYPE OF REPORT: Final

PREPARED FOR: U.S. Army Medical Research and Materiel Command
Fort Detrick, Maryland 21702-5012

REPORT DOCUMENTATION PAGE

Form Approved
OMB No. 0704-0188

1. REPORT DATE *(DD-MM-YYYY)*	**2. REPORT TYPE**	**3. DATES COVERED** *(From - To)*
01-08-2006	Final	30 Jul 2005 – 19 Jul 2006

4. TITLE AND SUBTITLE

Non-Invasive Phosphorus-31 Magnetic Resonance Spectral Characterization of Breast Tissue Anomalies Using Pattern Recognition and Artificial Intelligence

5a. CONTRACT NUMBER

5b. GRANT NUMBER
W81XWH-05-1-0491

5c. PROGRAM ELEMENT NUMBER

6. AUTHOR(S)
Jerry A. Darsey, Ph.D.; Diana Lindquist, Ph.D.; Dan Buzatu, Ph.D., et al.

E-Mail: jadarsey@ualr.edu

5d. PROJECT NUMBER

5e. TASK NUMBER

5f. WORK UNIT NUMBER

7. PERFORMING ORGANIZATION NAME(S) AND ADDRESS(ES)

University of Arkansas at Little Rock
Little Rock, Arkansas 72204-1099

8. PERFORMING ORGANIZATION REPORT NUMBER

9. SPONSORING / MONITORING AGENCY NAME(S) AND ADDRESS(ES)
U.S. Army Medical Research and Materiel Command
Fort Detrick, Maryland 21702-5012

10. SPONSOR/MONITOR'S ACRONYM(S)

11. SPONSOR/MONITOR'S REPORT NUMBER(S)

12. DISTRIBUTION / AVAILABILITY STATEMENT
Approved for Public Release; Distribution Unlimited

13. SUPPLEMENTARY NOTES

14. ABSTRACT

No abstract provided.

15. SUBJECT TERMS
No subject terms provided.

16. SECURITY CLASSIFICATION OF:			**17. LIMITATION OF ABSTRACT**	**18. NUMBER OF PAGES**	**19a. NAME OF RESPONSIBLE PERSON**
a. REPORT	**b. ABSTRACT**	**c. THIS PAGE**			USAMRMC
U	U	U	UU	15	**19b. TELEPHONE NUMBER** *(include area code)*

Table of Contents

Non-invasive Phosphorus-31 MR spectral characterization of *in vivo* breast tissue anomalies using pattern recognition and artificial intelligence (AI) techniques

I. Introduction:

It is highly desirable to develop a non-invasive spectroscopic and pattern recognition technique that can detect and reliably interpret images or spectral data from small volumes of the breast. Due to the pervasive nature of breast cancer in society today, and the consequent need of a highly accurate, early diagnostic tool, this is a very timely proposal that could have a significant impact on women's health. Patient ROtating Delivery of Excitation Off-resonance (RODEO) MRI data has been obtained from Dr. Diana Lindquist at the University of Arkansas for Medical Sciences. These patients, which flagged suspicious regions in breast tissue, have undergone needle biopsies from these suspect regions for pathological examination. With the patient's permission, Dr. Lindquist obtained P-31 MR scans of the flagged suspect tissue and healthy tissue in the same session. Access to data from 6 patients were obtained and made available for analysis in this study. We proposed to use a combination of pattern recognition techniques, including Artificial Neural Networks (ANN), to develop *in vivo* methods that use breast P-31 MR scans (suspicious and non-suspicious regions) to diagnose potential malignant tissue. The MR scan data will be paired with the known biopsy results to create a supervised training set. Unfortunately two events occurred to prevent us from completing this study[1-3].

First, originally we were to obtain data on 25 patients. However before all 25 patients were scanned, the MRI instrument used in this study was decommissioned for replacement by a more powerful and updated MRI. We successfully completed MRI P-31 scans on only six patients. The transition from old to new MRI required approximately 4 months. Second, the new MRI needed to have a new P-31 MRI probe constructed. Such a task requires expertise in probe design. The expert in this

project with this expertise, Dr. Diana Lindquist, took another job in Cincinnati, Ohio before she was able to develop a new probe for the new MRI.

For the reasons mentioned previously, it is highly desirable to develop a non-invasive spectroscopic and pattern recognition technique that can detect and reliably interpret images or spectral data from small volumes of the breast. Due to the pervasive nature of breast cancer in society today, and the consequent need of a highly accurate, early diagnostic tool, this is a very timely proposal that could have a significant impact on women's health. The results of the brain scan study suggest that breast tumor detection may be possible at a very early stage with this technique given sufficient examples in the training sets [4]. There is a high degree of correlation between the chance of complete eradication, recovery, and survival from cancer and how early it's detected. This is true for breast cancer as it is for all other types of cancer.

II Methods:

A. Subjects:

Seven patients were chosen because they had a suspicious mass found either by mammography or palpation and were scheduled for either surgery or biopsy. They were excluded if they had had a previous core biopsy from the site. The local institutional review board approved this study. A typical MRI instrument containing patient is shown in Figure 1a with corresponding schematic of important components shown in Figure 1b.

Figure 1a: Typical MRI instrument with a patient shown being readied for

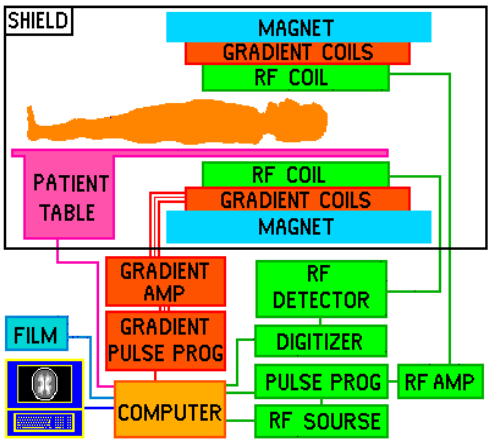

Figure 1b: Schematic of typical MRI instrument used . in this project.

MRI scan.

B. MR Data Acquisition

All data were acquired on a 1.5 T General Electric Signa Horizon system (General Electric, Milwaukee, WI, USA) using a home-built solenoid phosphorus coil placed inside a proton transmit/receive bilateral breast coil (MRI Devices, Milwaukee, WI, USA). For these studies, only one breast was examined, so the proton coil was operated as either a right- or left-only coil.

C. Phosphorus-31 coil:

The phosphorus coil consisted of ¼-inch wide copper tape wrapped on an acrylic tube 13.6 cm in diameter. The coil was 9 cm tall from top to bottom. The acrylic tube was fitted with a plastic flange to allow it to hang from the top of the proton breast coil. Variable capacitors were used for tuning and matching the coil, which was done for most of the subjects recruited. A balun was inserted in the coil cable to minimize effects from cable currents. Figure 2 below shows a typical MRI spectra from normal human tissue [1].

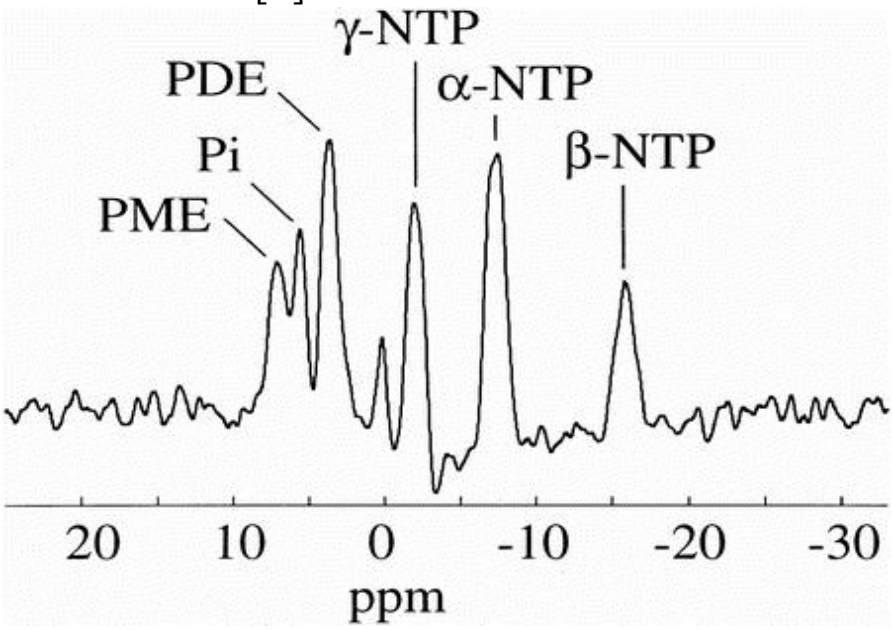

Figure 2. Example of a ^{31}P magnetic resonance spectrum from normal human tissue.

In this ^{31}P magnetic resonance spectrum from normal human tissue we see that the peak area is proportional to amount of metabolite. Peaks labeled on scan: PME, phosphomonoesters (mainly phospholipid precursors, principally phosphocompounds of choline and ethanolamine,

with some contribution from sugar phosphates); Pi, inorganic phosphate (product of ATP hydrolysis); PDE, phosphodiesters (phospholipid catabolites, mainly glycerophosphocompounds of choline and ethanolamine, with some contribution from cell membranes); and γ-, α-, β-phosphates of nucleotide triphosphates, NTP (high-energy phosphate compounds). By convention, the [β-P] NTP peak is taken to represent ATP. Phosphocreatine peak (not labeled) is at zero parts per million (assumed from muscle contamination). Data are conventionally presented as ratios of related peak areas, comprising phosphoester metabolites (PME/PDE) and energy status (ATP/Pi) respectively. Alternatively, individual peak areas may be expressed as a function of total visible phosphate (TP). These measures are independent of the volume of liver from which the signals are obtained. Liver intracellular pH (pHic) was derived from the chemical shift difference between [α-P] NTP, assigned to −7.5 ppm, and Pi, according to the supplied calibration data. ppm, resonance chemical shift in parts per million.

The phosphorus coil (see for example Figures 3 and 4)[2] was centered in the appropriate side of the proton coil and the subject was positioned prone on top of the coils with the breast to be examined hanging freely. The contralateral breast was compressed against the chest to minimize artifacts in the clinical images. The patient was then centered in the magnet (see Figure 1a). Pre- and post-contrast clinical RoDEO images were acquired to localize the lesion (parameters: flip angle: 45 degrees; repetition time 20ms; echo time 5ms; 128x256 matrix; slice thickness 1.4-1.8 mm; 128 slices). A slice containing the lesion was chosen and used as the center point for the spectroscopy exam. The spectroscopy exam used a phase-encoded pulse acquire technique (parameters: 25 degree flip angle, repetition time 300ms, 6 x 6 matrix, 512 complex points, 2000 Hz spectral width, 75 NEX, 200 mm FOV, and 30 mm slice thickness). Each spectral data set required about 30 minutes to acquire. To assess the reproducibility of the technique, spectra were acquired on three separate days from one volunteer. For all other subjects, spectra were acquired once.

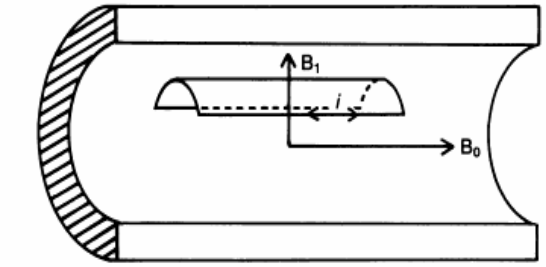

Figure 3. A saddle-shaped radio frequency (RF) coil inside a solenoid magnet. B_0=the direction of the magnetic field of the solenoidal magnet, B_1=the direction of the magnetic field produced by current flow, *i*, in the RF coil.

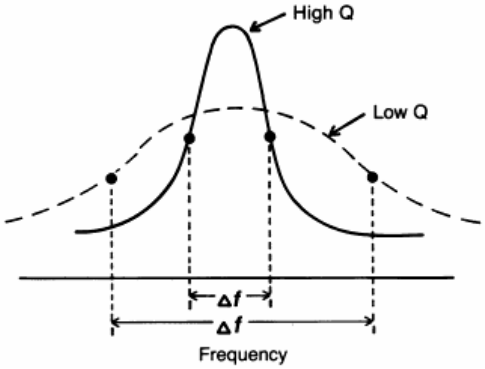

Figure 4. Dependence of bandwidth, Δf, of coil on value of Q.

Data were transferred to an off-line workstation (SGI O_2 system) for processing and analysis. The data were processed using SA/GE (Spectral analysis software, General Electric, Milwaukee, WI, USA). All data were given 10 Hz of exponential line-broadening prior to Fourier transformation. The data were phased automatically, with some manual phasing of individual spectra if needed. The phased spectra were overlaid on the central image from the clinical exam for display [5-7].

III Key Research Accomplishments:

- Ran MRIs on six patients using RoDEO enhancements to pinpoint potential breast tissue anomalies.
- Ran 36 voxels of data for P-31 spectra on all 6 patients.
- Thirty-six, 180 cm^3 voxels were obtained and the corresponding P-31 spectra were obtained for each MRI scan of each patient.
- The 36 spectra per patient were examined to locate the peaks from phosphomonoesters, phosphodiesters, phosphocreatine, inorganic phosphate, and the ATP peaks.
- Analysis was performed with AI software. The signal-to-noise ratio was too low to allow the unambiguous determination of either the location or intensity of any of these peaks [6,7].

IV. Reportable Outcomes:

The following are examples of both the MRI images of a breast (Figure 5a and Figure 6a) and the corresponding P-31 spectra (Figure 5b and Figure 6b)of the lesion which was targeted. The "aqua" spectra seen on the breast image is located in the area of the voxel where the P-31 spectra was obtained. Spectra were obtained for both normal (benign) tissue and potentially malignant tissue.

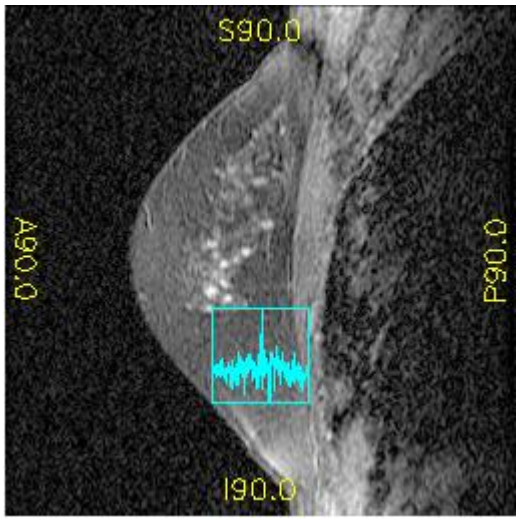

Figure 5a: MRI image of breast for Patient 1(normal tissue).

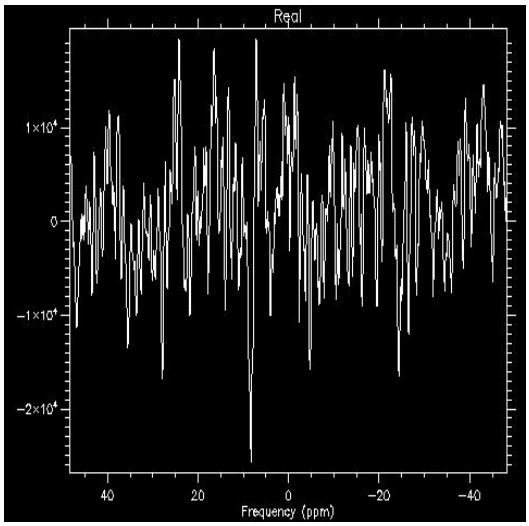

Figure 5b: P-31 spectra of breast on left for Patient 1.

The following figures (Figure 6a and 6b) show the MRI image and corresponding P-31 spectra for a patient with a diagnosed malignant tumor.

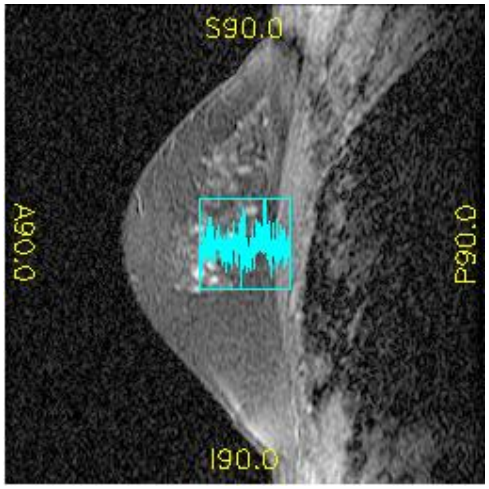

Figure 6a: MRI image of breast for Patient 2 (suspected malignant area)

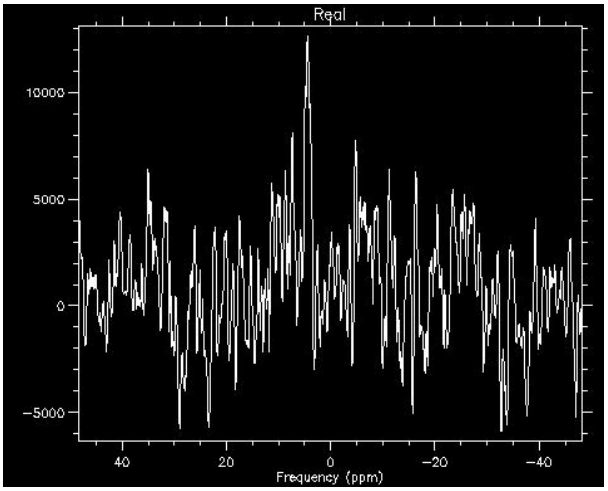

Figure 6b: P-31 spectra of breast on left for Patient 2.

The raw data from the phosphorus scan, as previously stated, was transferred to an SGI O_2 workstation for offline processing using the GE Spectral Analysis (SA/GE) package. The data was processed to achieve the best resolution and signal to noise ratios, which required zero-filling and apodizing the raw data prior to Fourier transformation. The precise processing parameters will be determined from the first data set and will be used consistently throughout this project. Initial processing parameters will be zero-filling once with 10 Hz exponential line broadening applied.

V. Conclusion and Summary:

With breast cancer being the number one cancer in woman with over 200,000 diagnosed this year, and more than 1.6 million women a survivor of this cancer, we strongly believe that the procedure outlined in this research proposal has the potential to provide a much earlier diagnosis which should reduce the need of biopsies, and, potentially provide a much higher cure rate due to this earlier detection and diagnosis [11,12].

Due to the limited number of patients we were able to recruit for this project it was not possible to perform sufficient artificial neural network analysis. We originally wanted to study at least 25 patients, of which at least half, or approximately 10 to 12 were diagnosed with a malignant tumor verified using a biopsy. However, we were only able to recruit 6 patients with only one patient (patient 2) having a confirmed malignant breast tumor. In addition, the Co-PI, Dr. Diana Lindquist, is no longer available for this project. She has accepted as of May,2006 another position in Cleveland, Ohio. Therefore we will not be able to perform any additional MRI scans with the accompanying P-31 spectra for analysis.

However, in discussions with Dr. Lindquist and other Co-PIs on the project, we will begin looking at in vitro tissue samples which have undergone a biopsy for the presence of malignant tissue. We will perform NMR P-31 spectral analysis on these tissue samples for analysis with ANN. We should be able to perform analysis on several hundred patient samples and compare these malignant samples with non-malignant samples.

VI. References:

[1] Mann,D.V., W. M. Lam, N. Magnus Hjelm, Nina M. C. So, David K. W. Yeung, C. Metreweli, Wan Y. Lau, "Metabolic Control Patterns in Acute Phase and Regenerating Human Liver Determined In Vivo by 31-Phosphorus Magnetic Resonance Spectroscopy", *Ann Surg*. 2002 March; 235(3): 408–416.

[2] Scherzinger, A.L. and William R. Hendee, "Basic Principles of Magnetic Resonance Imaging—An Update", *West J Med.* 1985 December; 143(6): 782–792.

[3] Ding, Y.-S., Kil, K.-E., Lin, K.-S., Ma, W., Yokota, Y. and Carroll, I. F. A Novel Nicotinic Acetylcholine Receptor Antagonist Radioligand Studies. Bioorgan. Med. Chem. Lett. 16, 1049-1053, 2006.

[4] Beger, R., Freeman J., Lay Jr. J., Wilkes J. and Miller, D. "^{13}C NMR and EI mass spectrometric data-activity relationship (SDAR) model of estrogen receptor binding." *Toxicology and Applied Pharmacolgy*. (2000), 169, 17-25

[5] Marsteller, D. A., Barbarich-Marsteller, N. C., Fowler, J. S., Schiffer, W. K., Alexoff, D. L., Rubins, D. and Dewey, S. L. Reproducibility of Intraperitoneal 2-deoxy-2-[18F]-fluoro-D-glucose Cerebral Uptake in Rodents Through Time. Nucl. Med. Biol. 33, 71-79, 2006.

[6] Schiffer, W. K., Volkow, N. D., Fowler, J. S., Alexoff, D. L., Logan, J. and Dewey, S. L. "Therapeutic Doses of Amphetamine and Methylphenidate Differentially Increase Synaptic and Extracellular Dopamine. Synapse 59, 243-251, 2006.

[7] Buzatu, D.A., Beger, R.D., Wilkes, J.G., Darsey, J.A., Klimbert, S. and Lindquist, D.M., "Non-Invasive Brain Tumor Diagnostic Models Developed from Proton Magnetic Resonance Spectroscopy using Novel Pattern Recognition Methods", *J. Mag. Res*. (submitted)

[8] Darsey J. A., Lay J. O., Holland R. D.; "Deconvolution of composite mass spectra using artificial neural networks",*Int. J. Chem. and Biotech.,* (1999) 17**,** No. 9, 41**.**

[9] Schnall M.D., "Application of magnetic resonance imaging to early detection of breast cancer." *Breast Cancer Res*., (2001), 3(1):17-21.

[10] Beger, R.D., Buzatu, D.A., Wilkes, J.G., and Lay, Jr., J.O. "Comparative Structural Connectivity Spectra Analysis (CoSCoSA) Models of Steroid Binding to the Corticosteroid Binding Globulin." *J. Chem. Inf. Comp. Sci.*, (2002) 42(5):1123-1131.

[11] D Kingsmore, A Ssemwogerere, D Hole and C Gillis "Specialisation and breast cancer survival in the screening era", *British Journal of Cancer, 88*,(2003), 1708.

[12] Parker, S.L., Tong, T., Bolden, S, et al.: Cancer statistics, 1996. *Ca-A Cancer Journal for Clinicians, 46*(1): 5-27, 1996.

VII Appendix:

Table 1. The following data is an example of MRI P-31 spectral data obtained from one run of one voxel from one patient. This is only one data set of 36 per patient.

-48.3372	-910.782	-3245.02	-48.3372	-910.782	-3245.02	-48.3372	-910.782	-3245.02
-48.2428	-1690.84	-2147.08	-48.2428	-1690.84	-2147.08	-48.2428	-1690.84	-2147.08
-48.1484	-1914.17	-1049.76	-48.1484	-1914.17	-1049.76	-48.1484	-1914.17	-1049.76
-48.054	-1688.97	173.7177	-48.054	-1688.97	173.7177	-48.054	-1688.97	173.7177
-47.9596	-622.148	1054.866	-47.9596	-622.148	1054.866	-47.9596	-622.148	1054.866
-47.8652	532.5189	938.0002	-47.8652	532.5189	938.0002	-47.8652	532.5189	938.0002
-47.7707	1215.161	453.6369	-47.7707	1215.161	453.6369	-47.7707	1215.161	453.6369
-47.6763	1648.259	-372.932	-47.6763	1648.259	-372.932	-47.6763	1648.259	-372.932
-47.5819	1159.117	-1339.67	-47.5819	1159.117	-1339.67	-47.5819	1159.117	-1339.67
-47.4875	131.9281	-1267.76	-47.4875	131.9281	-1267.76	-47.4875	131.9281	-1267.76
-47.3931	-48.5061	-412.905	-47.3931	-48.5061	-412.905	-47.3931	-48.5061	-412.905
-47.2987	604.1929	-197.056	-47.2987	604.1929	-197.056	-47.2987	604.1929	-197.056
-47.2043	710.0126	-685.19	-47.2043	710.0126	-685.19	-47.2043	710.0126	-685.19
-47.1099	334.7101	-699.416	-47.1099	334.7101	-699.416	-47.1099	334.7101	-699.416
-47.0155	234.1037	-402.606	-47.0155	234.1037	-402.606	-47.0155	234.1037	-402.606
-46.9211	401.9159	-60.7045	-46.9211	401.9159	-60.7045	-46.9211	401.9159	-60.7045
-46.8267	881.0281	20.64682	-46.8267	881.0281	20.64682	-46.8267	881.0281	20.64682
-46.7323	1203.557	-233.799	-46.7323	1203.557	-233.799	-46.7323	1203.557	-233.799
-46.6378	1443.263	-491.816	-46.6378	1443.263	-491.816	-46.6378	1443.263	-491.816
-46.5434	1641.428	-1032.7	-46.5434	1641.428	-1032.7	-46.5434	1641.428	-1032.7
-46.449	1343.275	-1658.83	-46.449	1343.275	-1658.83	-46.449	1343.275	-1658.83
-46.3546	899.7252	-1890.39	-46.3546	899.7252	-1890.39	-46.3546	899.7252	-1890.39
-46.2602	545.8783	-2253.32	-46.2602	545.8783	-2253.32	-46.2602	545.8783	-2253.32
-46.1658	-512.042	-2543.14	-46.1658	-512.042	-2543.14	-46.1658	-512.042	-2543.14
-46.0714	-1746.02	-1648.69	-46.0714	-1746.02	-1648.69	-46.0714	-1746.02	-1648.69
-45.977	-1805.84	-45.4079	-45.977	-1805.84	-45.4079	-45.977	-1805.84	-45.4079
-45.8826	-832.514	929.9805	-45.8826	-832.514	929.9805	-45.8826	-832.514	929.9805
-45.7882	242.5123	1167.244	-45.7882	242.5123	1167.244	-45.7882	242.5123	1167.244
-45.6938	1389.665	865.2434	-45.6938	1389.665	865.2434	-45.6938	1389.665	865.2434
-45.5994	2100.71	-268.273	-45.5994	2100.71	-268.273	-45.5994	2100.71	-268.273
-45.5049	1782.054	-1476.76	-45.5049	1782.054	-1476.76	-45.5049	1782.054	-1476.76
-45.4105	839.2883	-2021.62	-45.4105	839.2883	-2021.62	-45.4105	839.2883	-2021.62
-45.3161	57.37751	-1651.71	-45.3161	57.37751	-1651.71	-45.3161	57.37751	-1651.71
-45.2217	194.5479	-1175.96	-45.2217	194.5479	-1175.96	-45.2217	194.5479	-1175.96
-45.1273	488.801	-1497.75	-45.1273	488.801	-1497.75	-45.1273	488.801	-1497.75
-45.0329	98.8756	-2072.64	-45.0329	98.8756	-2072.64	-45.0329	98.8756	-2072.64
-44.9385	-791.473	-2049.57	-44.9385	-791.473	-2049.57	-44.9385	-791.473	-2049.57
-44.8441	-1161.86	-1294.43	-44.8441	-1161.86	-1294.43	-44.8441	-1161.86	-1294.43
-44.7497	-755.977	-988.529	-44.7497	-755.977	-988.529	-44.7497	-755.977	-988.529
-44.6553	-700.569	-1386.64	-44.6553	-700.569	-1386.64	-44.6553	-700.569	-1386.64
-44.5609	-1350.74	-1646.55	-44.5609	-1350.74	-1646.55	-44.5609	-1350.74	-1646.55
-44.4665	-2206.08	-1110.13	-44.4665	-2206.08	-1110.13	-44.4665	-2206.08	-1110.13
-44.372	-2266.56	-37.3928	-44.372	-2266.56	-37.3928	-44.372	-2266.56	-37.3928
-44.2776	-1668.78	436.3974	-44.2776	-1668.78	436.3974	-44.2776	-1668.78	436.3974
-44.1832	-1412.6	394.9462	-44.1832	-1412.6	394.9462	-44.1832	-1412.6	394.9462
-44.0888	-1379.66	561.672	-44.0888	-1379.66	561.672	-44.0888	-1379.66	561.672
-43.9944	-1136.29	649.5616	-43.9944	-1136.29	649.5616	-43.9944	-1136.29	649.5616

Table 1. (continued)

-43.8056	-1591.39	852.8599	-43.8056	-1591.39	852.8599	-43.8056	-1591.39	852.8599
-43.7112	-1388.02	1590.894	-43.7112	-1388.02	1590.894	-43.7112	-1388.02	1590.894
-43.6168	-634.574	1846.226	-43.6168	-634.574	1846.226	-43.6168	-634.574	1846.226
-43.5224	-182.489	1410.253	-43.5224	-182.489	1410.253	-43.5224	-182.489	1410.253
-43.428	-488.897	1076.503	-43.428	-488.897	1076.503	-43.428	-488.897	1076.503
-43.3335	-864.559	1542.665	-43.3335	-864.559	1542.665	-43.3335	-864.559	1542.665
-43.2391	-409.926	2175.018	-43.2391	-409.926	2175.018	-43.2391	-409.926	2175.018
-43.1447	157.087	2021.55	-43.1447	157.087	2021.55	-43.1447	157.087	2021.55
-43.0503	53.60254	1965.013	-43.0503	53.60254	1965.013	-43.0503	53.60254	1965.013
-42.9559	236.5543	2521.127	-42.9559	236.5543	2521.127	-42.9559	236.5543	2521.127
-42.8615	1067.008	2861.864	-42.8615	1067.008	2861.864	-42.8615	1067.008	2861.864
-42.7671	2035.068	2654.501	-42.7671	2035.068	2654.501	-42.7671	2035.068	2654.501
-42.6727	2928.347	1971.809	-42.6727	2928.347	1971.809	-42.6727	2928.347	1971.809
-42.5783	3358.361	679.5933	-42.5783	3358.361	679.5933	-42.5783	3358.361	679.5933
-42.4839	2812.034	-499.876	-42.4839	2812.034	-499.876	-42.4839	2812.034	-499.876
-42.3895	2078.374	-987.662	-42.3895	2078.374	-987.662	-42.3895	2078.374	-987.662
-42.2951	1373.647	-1403.6	-42.2951	1373.647	-1403.6	-42.2951	1373.647	-1403.6
-42.2006	286.4179	-1424.81	-42.2006	286.4179	-1424.81	-42.2006	286.4179	-1424.81
-42.1062	-555.958	-752.619	-42.1062	-555.958	-752.619	-42.1062	-555.958	-752.619
-42.0118	-935.479	172.0492	-42.0118	-935.479	172.0492	-42.0118	-935.479	172.0492
-41.9174	-711.475	1285.723	-41.9174	-711.475	1285.723	-41.9174	-711.475	1285.723
-41.823	243.7521	1887.929	-41.823	243.7521	1887.929	-41.823	243.7521	1887.929
-41.7286	1118.031	1723.481	-41.7286	1118.031	1723.481	-41.7286	1118.031	1723.481
-41.6342	1583.468	1243.045	-41.6342	1583.468	1243.045	-41.6342	1583.468	1243.045
-41.5398	1689.699	854.5495	-41.5398	1689.699	854.5495	-41.5398	1689.699	854.5495
-41.4454	1887.802	530.306	-41.4454	1887.802	530.306	-41.4454	1887.802	530.306
-41.351	1869.176	-115.247	-41.351	1869.176	-115.247	-41.351	1869.176	-115.247
-41.2566	1320.6	-613.754	-41.2566	1320.6	-613.754	-41.2566	1320.6	-613.754
-41.1621	548.4608	-553.633	-41.1621	548.4608	-553.633	-41.1621	548.4608	-553.633
-41.0677	169.6563	27.68352	-41.0677	169.6563	27.68352	-41.0677	169.6563	27.68352
-40.9733	287.343	482.1457	-40.9733	287.343	482.1457	-40.9733	287.343	482.1457
-40.8789	465.1859	643.5623	-40.8789	465.1859	643.5623	-40.8789	465.1859	643.5623
-40.7845	436.7585	800.9824	-40.7845	436.7585	800.9824	-40.7845	436.7585	800.9824
-40.6901	655.709	1258.421	-40.6901	655.709	1258.421	-40.6901	655.709	1258.421
-40.5957	1265.602	1291.614	-40.5957	1265.602	1291.614	-40.5957	1265.602	1291.614
-40.5013	1546.083	990.8132	-40.5013	1546.083	990.8132	-40.5013	1546.083	990.8132
-40.4069	1661.777	774.5599	-40.4069	1661.777	774.5599	-40.4069	1661.777	774.5599
-40.3125	1750.604	542.1177	-40.3125	1750.604	542.1177	-40.3125	1750.604	542.1177
-40.2181	1698.236	223.1239	-40.2181	1698.236	223.1239	-40.2181	1698.236	223.1239
-40.1237	1400.869	47.88004	-40.1237	1400.869	47.88004	-40.1237	1400.869	47.88004
-40.0292	1095.401	106.7472	-40.0292	1095.401	106.7472	-40.0292	1095.401	106.7472
-39.9348	785.3507	344.7289	-39.9348	785.3507	344.7289	-39.9348	785.3507	344.7289
-39.8404	581.1136	966.6189	-39.8404	581.1136	966.6189	-39.8404	581.1136	966.6189
-39.746	1094.592	1895.979	-39.746	1094.592	1895.979	-39.746	1094.592	1895.979
-39.6516	2400.454	2055.838	-39.6516	2400.454	2055.838	-39.6516	2400.454	2055.838
-39.5572	3264.755	1286.623	-39.5572	3264.755	1286.623	-39.5572	3264.755	1286.623
-39.4628	3576.869	486.9435	-39.4628	3576.869	486.9435	-39.4628	3576.869	486.9435
-39.3684	3654.662	-417.049	-39.3684	3654.662	-417.049	-39.3684	3654.662	-417.049
-39.274	3095.014	-1304.43	-39.274	3095.014	-1304.43	-39.274	3095.014	-1304.43
-39.1796	2165.288	-1392.04	-39.1796	2165.288	-1392.04	-39.1796	2165.288	-1392.04

Table 1. (continued)

-39.0852	1868.401	-851.317	-39.0852	1868.401	-851.317	-39.0852	1868.401	-851.317
-38.9907	2328.221	-664.094	-38.9907	2328.221	-664.094	-38.9907	2328.221	-664.094
-38.8963	2662.348	-1368.09	-38.8963	2662.348	-1368.09	-38.8963	2662.348	-1368.09
-38.8019	2035.069	-2134.88	-38.8019	2035.069	-2134.88	-38.8019	2035.069	-2134.88
-38.7075	1126.071	-2161.85	-38.7075	1126.071	-2161.85	-38.7075	1126.071	-2161.85
-38.6131	427.0704	-1735.19	-38.6131	427.0704	-1735.19	-38.6131	427.0704	-1735.19
-38.5187	117.3701	-998.099	-38.5187	117.3701	-998.099	-38.5187	117.3701	-998.099
-38.4243	270.3219	-340.054	-38.4243	270.3219	-340.054	-38.4243	270.3219	-340.054
-38.3299	605.017	152.7145	-38.3299	605.017	152.7145	-38.3299	605.017	152.7145
-38.2355	1298.704	543.0816	-38.2355	1298.704	543.0816	-38.2355	1298.704	543.0816
-38.1411	2218.775	161.337	-38.1411	2218.775	161.337	-38.1411	2218.775	161.337
-38.0467	2298.62	-648.663	-38.0467	2298.62	-648.663	-38.0467	2298.62	-648.663
-37.9523	2065.599	-883.108	-37.9523	2065.599	-883.108	-37.9523	2065.599	-883.108
-37.8578	2018.563	-1031.5	-37.8578	2018.563	-1031.5	-37.8578	2018.563	-1031.5
-37.7634	1994.053	-1019.03	-37.7634	1994.053	-1019.03	-37.7634	1994.053	-1019.03
-37.669	2434.039	-1078.69	-37.669	2434.039	-1078.69	-37.669	2434.039	-1078.69
-37.5746	2926.522	-1836.27	-37.5746	2926.522	-1836.27	-37.5746	2926.522	-1836.27
-37.4802	2797.235	-3020.37	-37.4802	2797.235	-3020.37	-37.4802	2797.235	-3020.37
-37.3858	1955.65	-4154.11	-37.3858	1955.65	-4154.11	-37.3858	1955.65	-4154.11
-37.2914	404.4081	-4773.69	-37.2914	404.4081	-4773.69	-37.2914	404.4081	-4773.69
-37.197	-1253.91	-4391.2	-37.197	-1253.91	-4391.2	-37.197	-1253.91	-4391.2
-37.1026	-2350.22	-3401.23	-37.1026	-2350.22	-3401.23	-37.1026	-2350.22	-3401.23
-34.7424	3228.471	-2040.56	-34.7424	3228.471	-2040.56	-34.7424	3228.471	-2040.56
-34.648	3100.886	-3279.93	-34.648	3100.886	-3279.93	-34.648	3100.886	-3279.93
-34.5535	1600.654	-4325.02	-34.5535	1600.654	-4325.02	-34.5535	1600.654	-4325.02
-34.4591	-486.409	-3841.55	-34.4591	-486.409	-3841.55	-34.4591	-486.409	-3841.55
-34.3647	-1738.76	-1897.63	-34.3647	-1738.76	-1897.63	-34.3647	-1738.76	-1897.63
-34.2703	-1260.44	472.7027	-34.2703	-1260.44	472.7027	-34.2703	-1260.44	472.7027
-34.1759	703.5732	1766.938	-34.1759	703.5732	1766.938	-34.1759	703.5732	1766.938
-34.0815	2688.591	1443.014	-34.0815	2688.591	1443.014	-34.0815	2688.591	1443.014
-33.9871	3933.663	426.366	-33.9871	3933.663	426.366	-33.9871	3933.663	426.366
-33.8927	4650.686	-1056.43	-33.8927	4650.686	-1056.43	-33.8927	4650.686	-1056.43
-33.7983	4258.882	-2612.09	-33.7983	4258.882	-2612.09	-33.7983	4258.882	-2612.09
-33.7039	3496.437	-3301.98	-33.7039	3496.437	-3301.98	-33.7039	3496.437	-3301.98
-33.6095	2949.12	-3946.55	-33.6095	2949.12	-3946.55	-33.6095	2949.12	-3946.55
-33.5151	1877.297	-4492.99	-33.5151	1877.297	-4492.99	-33.5151	1877.297	-4492.99
-33.4206	579.0143	-4356.7	-33.4206	579.0143	-4356.7	-33.4206	579.0143	-4356.7
-33.3262	-573.111	-3364.94	-33.3262	-573.111	-3364.94	-33.3262	-573.111	-3364.94
-33.2318	-498.53	-1619.73	-33.2318	-498.53	-1619.73	-33.2318	-498.53	-1619.73
-33.1374	984.8907	-942.968	-33.1374	984.8907	-942.968	-33.1374	984.8907	-942.968
-33.043	1890.062	-1726.66	-33.043	1890.062	-1726.66	-33.043	1890.062	-1726.66
-32.9486	1781.755	-2332.74	-32.9486	1781.755	-2332.74	-32.9486	1781.755	-2332.74
-32.8542	1768.243	-2494.29	-32.8542	1768.243	-2494.29	-32.8542	1768.243	-2494.29
-32.7598	1813.553	-2827.02	-32.7598	1813.553	-2827.02	-32.7598	1813.553	-2827.02
-32.6654	1756.955	-3052.58	-32.6654	1756.955	-3052.58	-32.6654	1756.955	-3052.58